DEEP H I SURVEY OF THE SPIRAL GALAXY NGC 2403

FILIPPO FRATERNALI

Instituto di Radioastronomia, CNR, via Gobetti 101, I-40129 Bologna, Italy; and Osservatorio Astronomico, Bologna, Italy;
ffratern@ira.bo.cnr.it

GUSTAAF VAN MOORSEL

National Radio Astronomy Observatory, P.O. Box O, Socorro, NM 87801; gvanmoor@aoc.nrao.edu

RENZO SANCISI

Osservatorio Astronomico, via Ranzani 1, I-40127 Bologna, Italy; and Kapteyn Astronomical Institute, University of Groningen, Netherlands;
sancisi@bo.astro.it

AND

TOM OOSTERLOO

ASTRON, Postbus 2, NL-7990 AA Dwingeloo, Netherlands; oosterloo@nfra.nl

ABSTRACT

High-sensitivity H I observations of the nearby spiral galaxy NGC 2403 obtained with the VLA are presented and discussed. The properties of the extended, differentially rotating H I layer with its H I holes, spiral structure, and outer warp are described. In addition, these new data reveal the presence of a faint, extended, and kinematically anomalous component. This shows up in the H I line profiles as extended wings of emission toward the systemic velocity. In the central regions these wings are very broad (up to 150 km s^{-1}) and indicate large deviations from circular motion. We have separated the anomalous gas component from the cold disk and have obtained for it a separate velocity field and a separate rotation curve. The mass of the anomalous component is 1/10 of the total H I mass. The rotation velocity of the anomalous gas is 25–50 km s^{-1} lower than that of the disk. Its velocity field has nonorthogonal major and minor axes that we interpret as due to an overall inflow motion of 10–20 km s^{-1} toward the center of the galaxy. The picture emerging from these observations is that of a cold H I disk surrounded by a thick and clumpy H I layer characterized by slower rotation and inflow motion toward the center. The origin of this anomalous gas layer is unclear. It is likely, however, that it is related to the high rate of star formation in the disk of NGC 2403 and that its kinematics is the result of a galactic fountain–type of mechanism. We suggest that these anomalous H I complexes may be analogous to a part of the high-velocity clouds of our Galaxy.

Key words: galaxies: halos — galaxies: individual (NGC 2403) — galaxies: ISM —
galaxies: kinematics and dynamics — galaxies: structure

1. INTRODUCTION

In recent years the study of the vertical structure and kinematics of the H I disks of spiral galaxies has been pursued almost exclusively with observations of galaxies viewed either edge-on or face-on. The study of edge-on systems has revealed vertical extensions of the H I layer up to several kiloparsecs from the plane and, in the case of NGC 891, also a slower rotation velocity of the gas in the halo (Swaters, Sancisi, & Van der Hulst 1997). In the face-on or nearly face-on galaxies the observations have shown vertical motions of neutral gas frequently associated with "holes" in the H I distribution (Puche et al. 1992; Kamphuis 1993). These results point at a substantial gas circulation between disk and halo (review by Sancisi 1999). The ejection of gas out of the disk is thought to be related to star formation in the disk and to be due to stellar winds and supernova explosions that blow out ionized gas. After cooling, this gas falls down to the plane. Such processes are generally described as *galactic fountains* (Shapiro & Field 1976; Bregman 1980). There are cases, however, in which the vertical motions originate from external events, such as collisions with intergalactic clouds and with small companions (van der

Hulst & Sancisi 1988). Accretion of intergalactic "primordial" gas, as proposed for the high-velocity clouds in our Galaxy (Oort 1970), may also play a role.

The present study represents a first attempt to use objects at intermediate inclination angles, which offer the advantage that, for a given object, information is obtained on both the density structure and the kinematics of H I in the vertical direction. The nearby spiral galaxy NGC 2403 is a suitable candidate because of its inclination angle of ∼60° and also because of its extended H I layer (about twice the optical size), its regular kinematics, and its symmetric, flat rotation curve. NGC 2403 is an isolated Sc III galaxy (Fig. 1) with a bright optical disk of about 8 kpc diameter surrounded by outer, faint surface brightness "fossil arms" (Sandage, Tammann, & Van den Bergh 1981). It hosts rich H II regions with brightnesses comparable to that of the 30 Doradus complex (Drissen et al. 1999).

Previous H I observations with the Westerbork Synthesis Radio Telescope (WSRT, Begeman 1987; Sicking 1997; Schaap, Sancisi, & Swaters 2000) of NGC 2403 showed systematic asymmetries in the H I velocity profiles along the major axis in the form of wings on the side of the lower rotation velocities, toward systemic. This
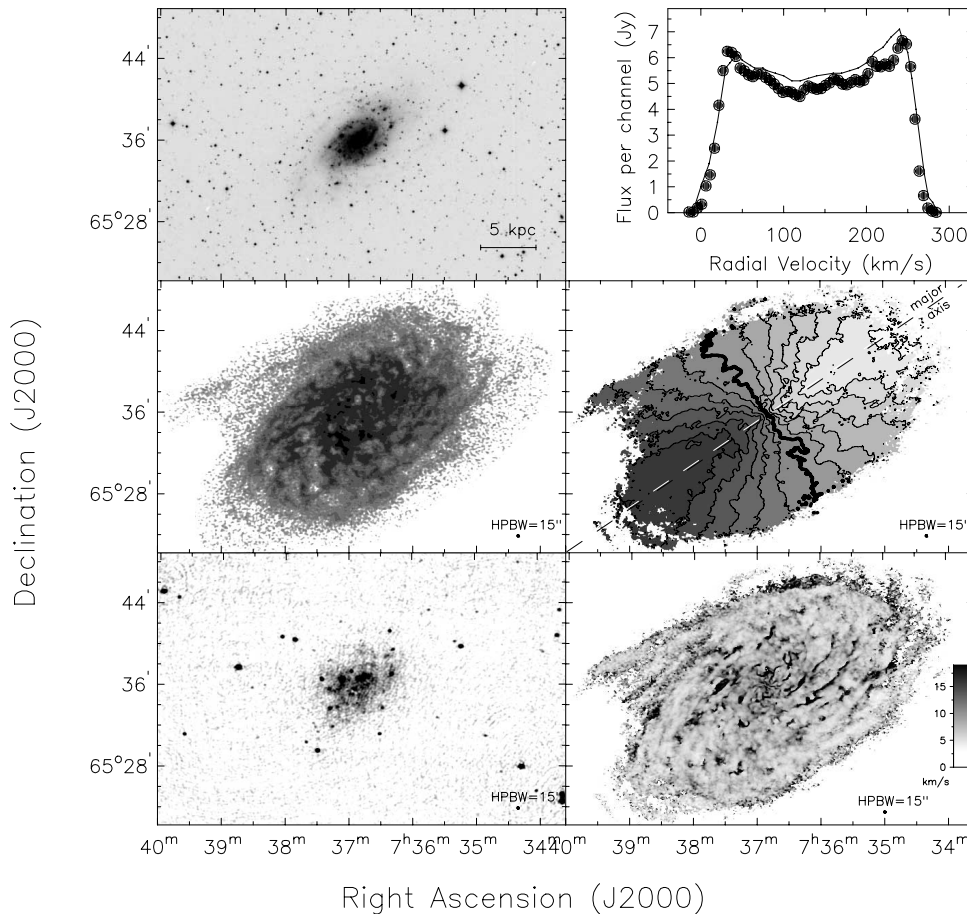
Fig. 1.—*From top left*: Optical image (DSS) of NGC 2403, global H I profile (*dots*) compared with previous single-dish observations (*line*) by Rots (1980), total H I map, velocity field, radio continuum, and velocity dispersion field. These are all at full resolution (15″). The column density in the total H I map ranges from 1×10^{20} to 5×10^{21} cm^{-2}. In the velocity field (*middle right*) the contours are separated by 20 km s^{-1}, and the thicker line marks the systemic velocity (133 km s^{-1}). The receding side is darker.

pattern (we refer to it as "the beard") is similar to that found in galaxies viewed edge-on or observed with low angular resolution but it is totally unexpected in NGC 2403 if its H I disk is thin. Schaap et al. (2000) reanalyzed Sicking's (1997) observations of NGC 2403 and investigated the effect of the layer thickness in order to explain such a pattern. They concluded that the beard may be produced by H I gas located above the plane (in a thick disk or halo) and rotating more slowly than the disk. Their picture is very similar to that proposed by Swaters et al. (1997) for NGC 891.

We obtained new H I observations of NGC 2403 with the Very Large Array.[1] These have led to a considerable improvement of the observational picture and to the detection of new, very faint emission from H I with remarkably anomalous kinematics.

2. OBSERVATIONS

We have observed NGC 2403 with the CS configuration of the VLA on four separate days in 1999 January and

February. This configuration differs from the regular C array in that the middle (fifth) telescope on the north arm is located at the innermost north arm location of the D array. This leads to a spatial resolution similar to that of the regular C array, while adding short baselines—and hence sensitivity at larger angular scales—not found in regular C-array observations (Rupen 1998). Each observation was 12 hours in duration, of which approximately 10 hours were spent on source. The remaining time was used to observe one phase calibrator (0841+708) and three flux calibrators (3C48, 3C147, and 3C28). The latter were used for bandpass calibration as well. The observational parameters are summarized in Table 1.

2.1. *Data Reduction*

Calibration and editing of the data were done separately for each of the four data sets, using standard procedures of the Astronomical Image Processing System (AIPS) package. Nineteen channels at both ends of the band (excluding the very edges) were identified as being free of line emission. The AIPS task UVLIN (Cornwell, Uson, & Haddad 1992) was then used to interpolate this continuum emission across the range of channels containing line emission and subtract it from the *uv* data.

TABLE 1
OBSERVATIONAL PARAMETERS FOR NGC 2403

Parameter	NGC 2403
Observation dates	1999 Jan 1, 28, 31; Feb 1
Length of observation (hr)	48
Time on source (hr)	40
Configuration	CS
Number of antennas	27
Pointing R.A. (J2000.0)..........	07 36 54.5
Pointing decl. (J2000.0)	+65 35 20.0
Central velocity (km s^{-1})........	130
Central frequency (MHz).......	1419.747
Total bandwidth (MHz).........	3.125
Total bandwidth (km s^{-1})	660
Number of channels	127
Channel separation (kHz)	24.4
Channel separation (km s^{-1}) ..	5.1

NOTE.—Units of right ascension are hours, minutes, and seconds, and units of declination are degrees, arcminutes, and arcseconds .

TABLE 2
PARAMETERS OF THE DATA CUBES

Parameter	Full Resolution	Smoothed
Used value of ROBUST............	0.2	0
Used taper (arcsec)...................	No taper	27
HPBW (arcsec)	15.2×13.3	29.7×29.3
P.A. of synthesized beam(deg)...	91.7	98.7
Beam size (pc)	234×205	458×452
Number of channels..................	62	62
rms noise per channel:		
No Hanning smoothing		
(mJy beam^{-1})	0.28	0.35
Hanning smoothing		
(mJy beam^{-1})	0.17	0.22
Minimum detectable column density:		
(cm^{-2})	5.0×10^{19}	2.0×10^{19}
($M_\odot$ pc^{-2}).............................	0.38	0.15
Minimum detectable mass		
($M_\odot$ beam^{-1})	2.1×10^4	2.6×10^4
Conversion factor (mJy K^{-1})	3.0	0.7

The resulting continuum-free *uv* data set containing the combined data for all four days was then further reduced using the Multichannel Image Reconstruction, Image Analysis, and Display (MIRIAD) package. The data cube was made using ROBUST or Briggs' weighting (Briggs 1995) with robustness 0.2 getting a spatial resolution of $\sim15''$ or 230 pc at the adopted distance of 3.18 Mpc (Madore & Friedman 1991). Another data cube was made by applying a Gaussian taper in the visibility domain. This data cube has a spatial resolution of $\sim30''$. The two cubes have 62 channels ranging in velocity from -24.7 km s^{-1} to 289.6 km s^{-1} and spaced by 5.15 km s^{-1}. To these data a Hanning smoothing was applied in velocity, leading to a velocity resolution of 10.3 km s^{-1}. The dirty images were deconvolved using a Clark CLEAN algorithm (Clark 1980). To identify the region of emission, the cubes were first CLEANed with a cutoff of 3 times the rms noise. The resulting images were then used to interactively define the regions of line emission in each channel. Next, a deep CLEAN (cutoff of $\sim0.2 \sigma$) was performed.

After cleaning, a few channel maps still showed some spurious effects (Fig. 2, *top left corner*, maps from 217.5 to 248.4 km s^{-1}). These may indicate the presence of very extended H I associated with the outer parts of the warp. Some channel maps show serious contamination from H I emission from our Galaxy at velocities around 0 km s^{-1} (Fig. 2, see the channel maps between about -10 km s^{-1} and about $+10$ km s^{-1}). This contamination is slightly reduced by applying the Hanning smoothing and also by using high-resolution data, because it generally has a greater angular scale than the emission from NGC 2403.

Comparison of our global H I profile with a previous single-dish profile from Rots (1980) (Fig. 1) shows we are not missing significant H I flux due to missing short spacings. The final data cube at $\sim15''$ resolution has an rms noise per channel of 0.17 mJy beam^{-1}, while the lower resolution data cube has an rms noise of 0.22 mJy beam^{-1}. The minimum detectable column density (5 σ detection in one velocity resolution element in the $30''$ resolution cube) is 2.0×10^{19} cm^{-2} (0.15 $M_\odot$ pc^{-2}) corresponding to $\sim2.6 \times 10^4$ $M_\odot$ beam^{-1}. This very high sensitivity has permitted us to detect very faint components in the neutral hydrogen that were not

seen in previous observations. A summary of the parameters for the two cubes is given in Table 2.

2.2. Data Description

Once the data cubes were obtained, the subsequent analysis was done using the Groningen Image Processing System (GIPSY) package. Figure 2 shows every second channel map of the $30''$ resolution cube of NGC 2403. We present here the smoothed data because they show more clearly the faint H I components. Some representative channels at high ($15''$) resolution are shown in Figure 8, overlaid on an optical DSS image. We also present several position-velocity (*p-v*) diagrams parallel to the major (Fig. 3) and minor (Fig. 4) axes. The cuts are shown in Figure 5 overlaid on the total H I map.

The full-resolution total H I map (Fig. 1) was obtained by adding the channel maps containing H I emission (from -19.6 to 279.3 km s^{-1}). For each channel map the areas with H I emission were outlined using masks made on the $30''$ resolution smoothed data cube. The total H I mass, corrected for the primary beam attenuation, is $3.24 \pm 0.05 \times 10^9$ $M_\odot$. The value of the mass derived for this galaxy by Begeman (1987) was 3.0×10^9 $M_\odot$, while Sicking (1997), with more sensitive observations, derived 3.13×10^9 $M_\odot$, assuming the distance of 3.18 Mpc. For comparison the single-dish mass (Rots 1980) is 3.31×10^9 $M_\odot$.

To first order, the distribution and the kinematics of the H I are regular. Figure 6 (*left*) shows the total H I at low ($60''$) resolution overlaid on the DSS optical image. The radius of the H I disk down to a column density of ~0.2 $M_\odot$ pc^{-2} (2.5×10^{19} cm^{-2}) is about 22 kpc (the Holmberg radius is 13 kpc). The H I disk appears to be full of holes, some having kiloparsec sizes (Mashchenko, Thilker, & Braun 1999). The very outer layer is warped. The warp is highly asymmetric, more pronounced on the eastern side of the galaxy (see channels from 176.2 to 227.8 km s^{-1}) than on the western side, where it is just faintly visible (channels from 42.3 to 62.9 km s^{-1}). The warp is also visible in the total H I map and in the velocity field at low resolution shown in Figure 6, where the H I disk on the northeast side appears to be more
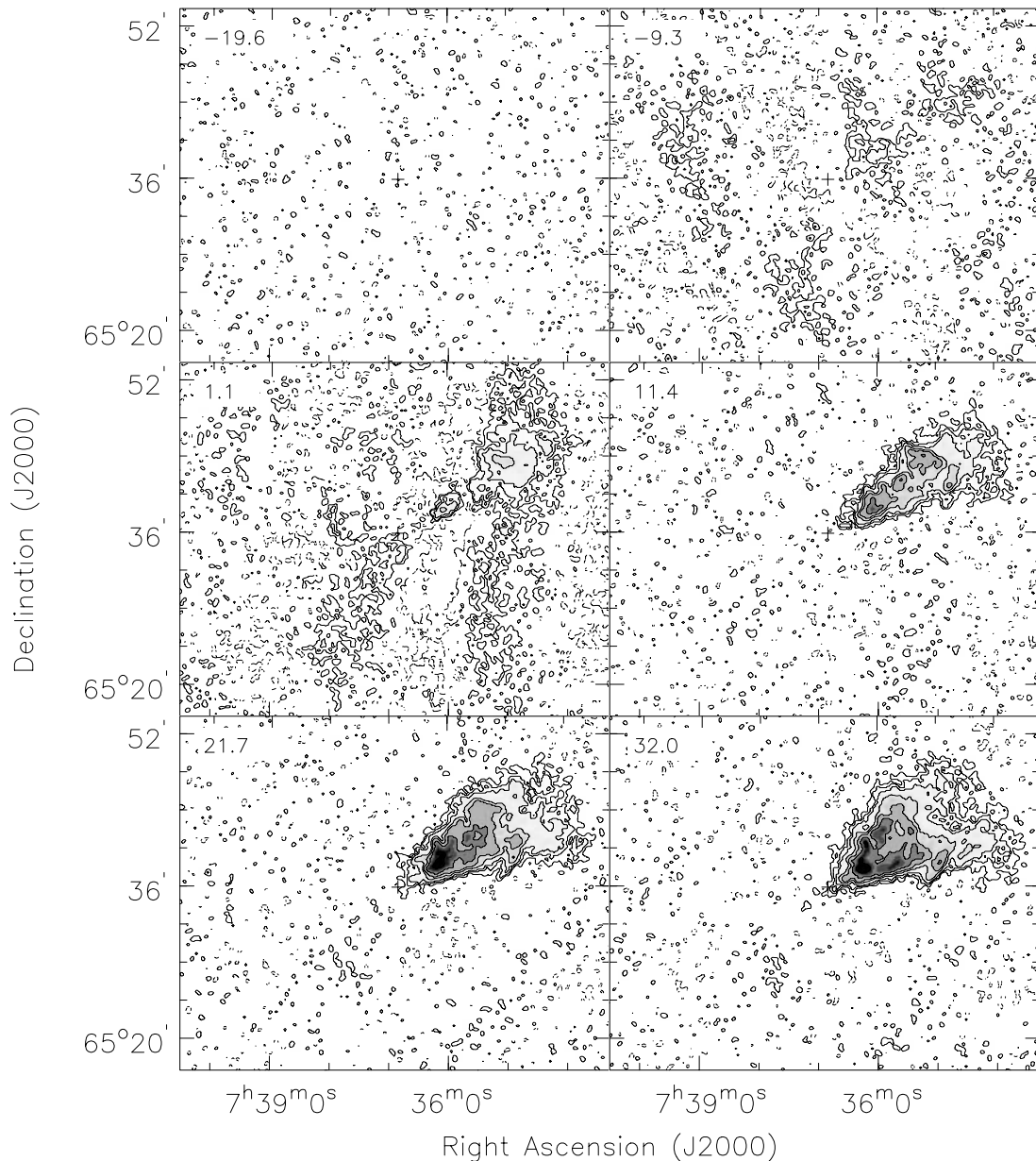
FIG. 2.—H I channel maps at 30″ resolution (Hanning-smoothed). The heliocentric radial velocities (km s^{-1}) are shown in the upper left corners. The contours are −0.5, 0.5, 1, 2, 5, 10, 20, 50 mJy beam^{-1}; the rms noise is 0.22 mJy beam^{-1}. The cross indicates the kinematical center of the galaxy.

extended. A summary of the optical and H i parameters for NGC 2403 is given in Table 3.

2.2.1. The Anomalous Gas

The most striking characteristics of the kinematics of the neutral hydrogen in NGC 2403 are illustrated in Figure 7. This diagram offers a display of the H I emission along the major axis of NGC 2403. It was obtained by integrating the 15″ full-resolution data over a slice 1′ wide in order to improve the signal-to-noise ratio. Clearly, the H I line profiles are strongly asymmetric with respect to the peak of the line emission. Note that the white squares, which mark the rotation curve, follow closely the ridge of the H I. There are H I tails extending (as a beard) toward the systemic velocity. The brighter of these tails had been seen in previous 21 cm

observations with the WSRT and already reported by Schaap et al. (2000). Because of the higher sensitivity of the present observations the tails are now much easier to recognize and they appear to extend over a much larger region of the position-velocity map. A clearer picture of the extent, the structure and the kinematics of the gas in the beard is now emerging. The density distribution is characterized by substructures in the form of filaments and spurs. These are observed all over the H I disk at velocities that differ by tens of kilometers per second from rotation. The most remarkable filament has a size of ~8 kpc and is visible in the channel maps between 93.8 and 155.6 km s^{-1}. It has a coherent structure and kinematics and its total H I mass is ~1 × 10^7 $M_\odot$. It does not show any obvious relation with any feature in the optical disk (Fig. 8, *top right and bottom left*) or with the H I spiral arms. The −1′ and −2′ *p-v* plots parallel to the
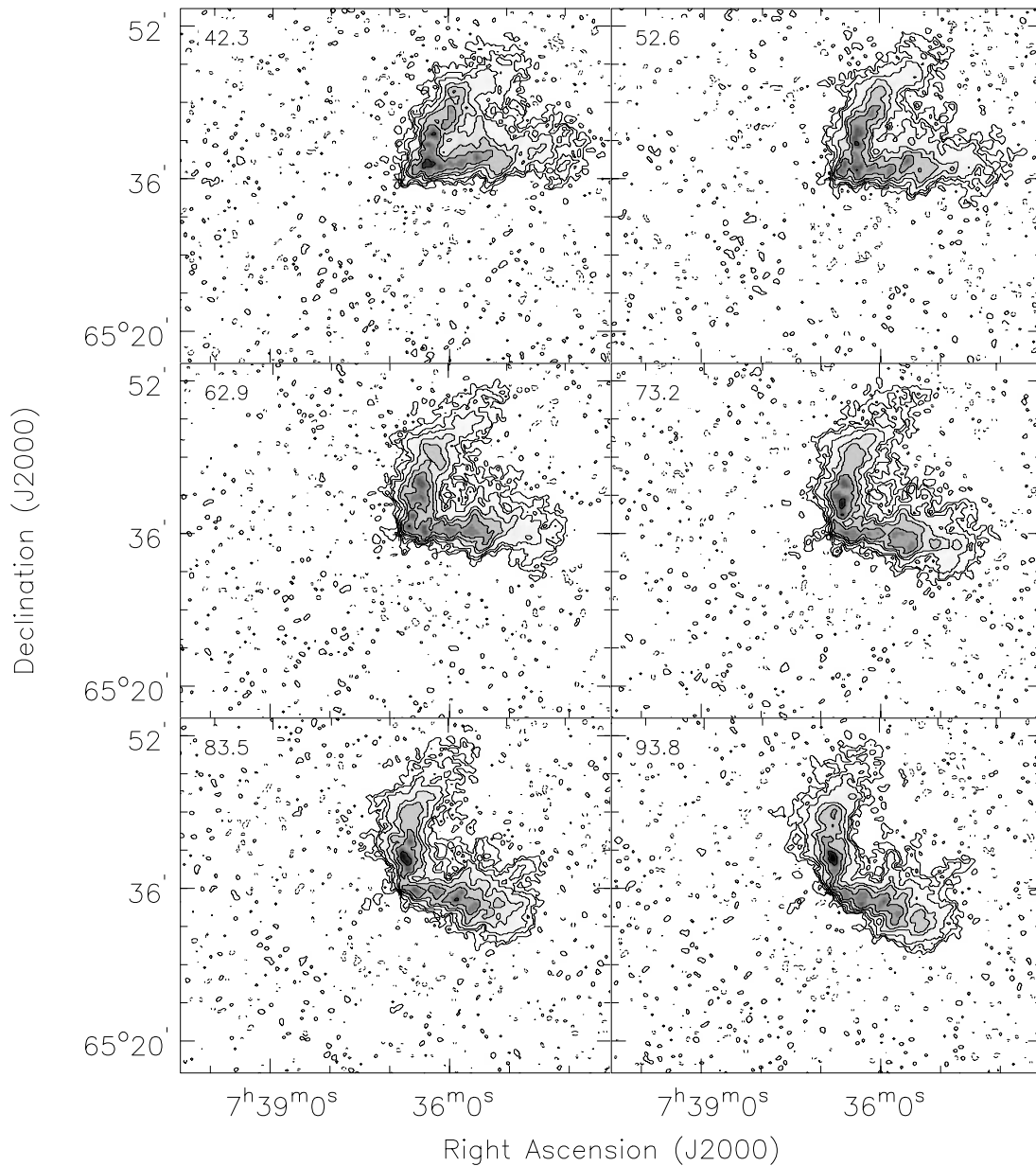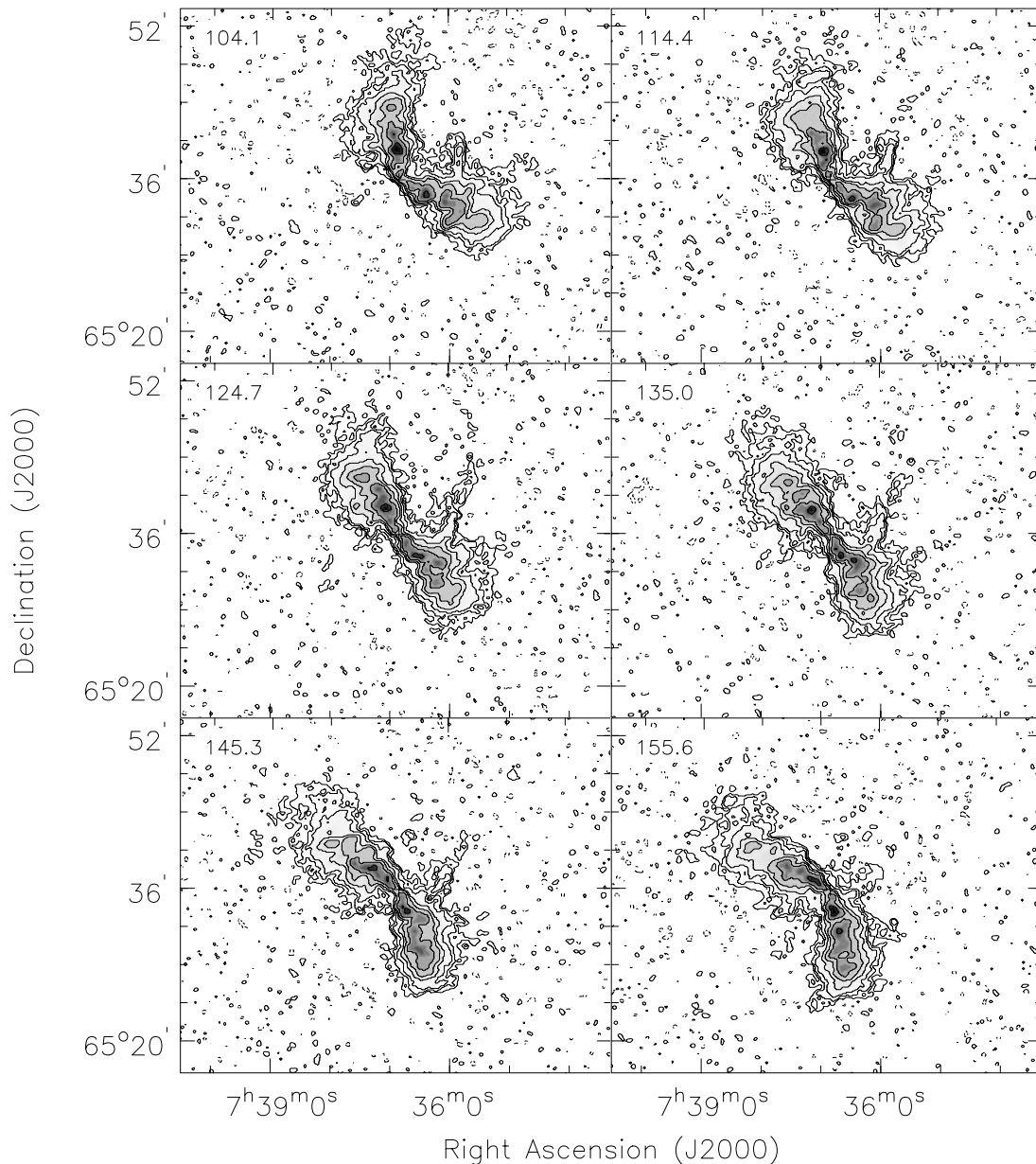
Fig. 2.—*Continued*

major axis (and partly also that along the major axis itself) in Figure 3 show this filament elongated on the low-velocity side between $0'$ and $-8'$. Remarkably, it follows the overall pattern of the low-density gas, suggesting that it is just a prominent condensation of gas within it and not a separate feature.

The *p-v* plots parallel to the minor axis (Fig. 4) show an asymmetric distribution of the low-level emission (tracing the beard). In the diagrams from $-4'$ to $-1'$, at velocities below the systemic velocity (horizontal line at 133 km s^{-1}), this low-level emission appears preferentially in the left part of the diagrams, between $0'$ and about $+10'$ (northeast side of the galaxy), whereas at velocities above systemic it is more visible in the right part of the plots. In the diagrams from $+1'$ to $+4'$, at velocities above systemic, the low-level emission is more prominent on the right part of the diagrams; at velocities below systemic it is in the left part. A

similar asymmetric distribution of the low-level H I emission is also seen in the channel maps close to the systemic velocity (Fig. 2), where the lower contours do not follow the H I ridge and seem displaced counter-clockwise. This effect indicates a rotation of the kinematical axes of the faint emission with respect to the axes of the cold disk. As we will discuss later (see § 3.2.1), such a change in the kinematical position angles can be attributed to an overall radial motion of the anomalous gas of about 10–20 km s^{-1} toward the center of the galaxy.

Apart from the extended low-level emission described above, the *p-v* diagrams in Figures 3 and 7 also show emission in the forbidden quadrants. This is particularly clear in the top right quadrant in Figure 7 ($0'$ to $-4'$ northwest with respect to the center) along the major axis at projected velocities (around 200 km s^{-1}), which differ from rotation by more than 130 km s^{-1}. The spatial loca-
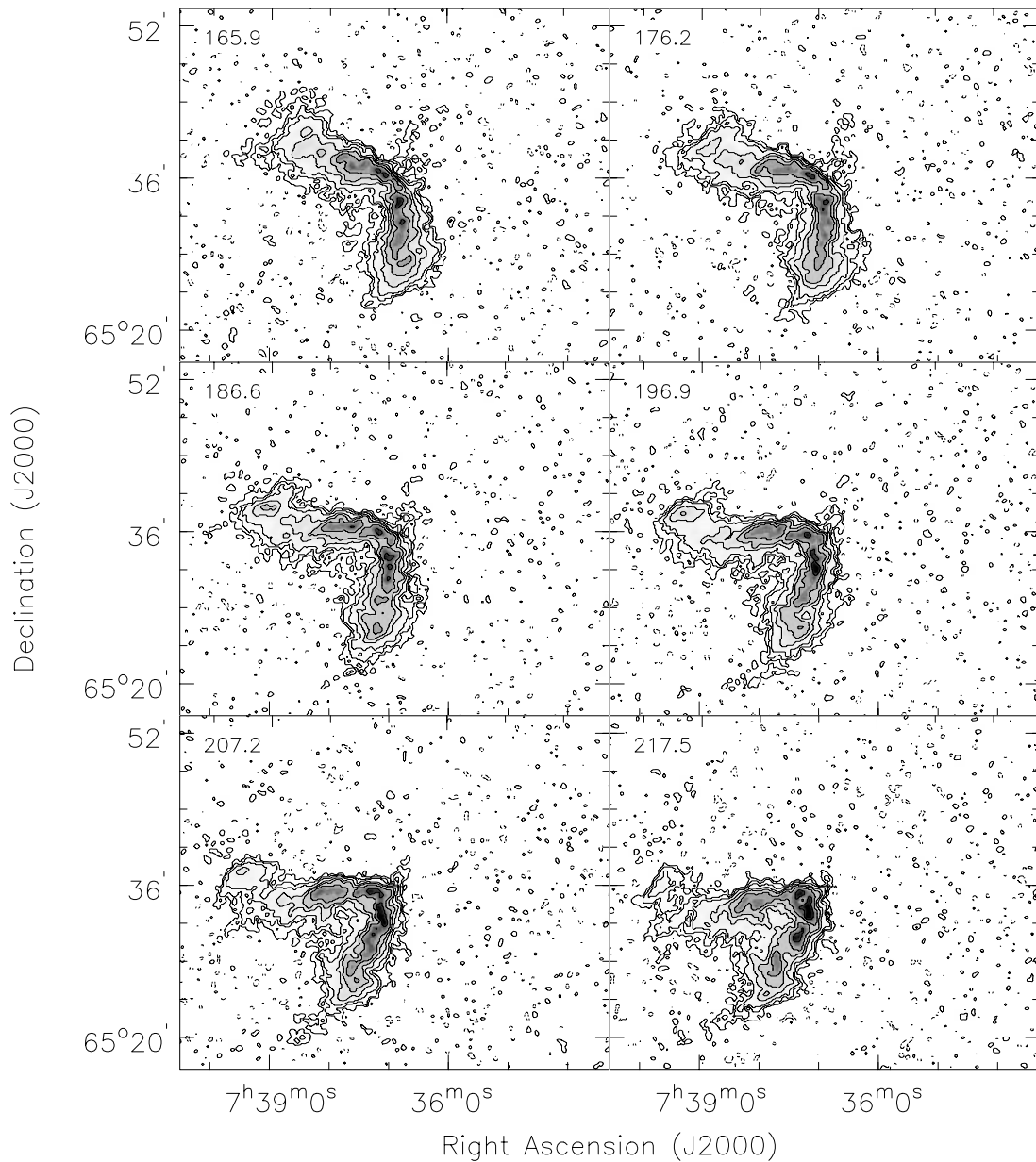
Fig. 2.—*Continued*

tion of this gas can be seen in the channel maps between 165.9 and 217.5 km s^{-1}, where it is visible just northwest of the center. The total mass of this gas is 4.3×10^6 $M_\odot$. The channel maps between 62.9 and 104.1 km s^{-1} show a faint counterpart on the southeast side of the galaxy, with a total mass of 1.7×10^6 $M_\odot$. All this gas at extreme anomalous velocities (the "forbidden" gas) seems to be confined to the region corresponding to the bright optical part of NGC 2403 (see Fig. 8, *top left and bottom right*). Its overall kinematical pattern, as it appears in Figure 7, indicates that all the anomalous gas, including the forbidden gas, forms one coherent structure, which closely follows the rotation of the system.

In the following we refer to all the gas at projected anomalous velocities with respect to the rotation curve (beard + anomalous gas).

3. THE SEPARATION OF THE ANOMALOUS GAS

We have attempted to separate the anomalous from the regular H I, assuming that the H I profiles are formed by two components: (1) a narrow one of Gaussian shape centered on the rotation velocity of the galaxy (the cold disk) and (2) a broader one, mainly at lower rotation velocities and with unknown profile shape (the anomalous gas). We have modeled the cold disk by fitting a Gaussian function to the line profile after clipping the data at 30% of the peak. With this clipping we fitted only the upper part of the profiles. The differences between the Gaussian fit with and without the clipping are about 1 km s^{-1} for the value of the rotation velocity and about 3 km s^{-1} for the velocity dispersion. The velocity field and the distribution of the velocity dispersion of the cold disk (Fig. 1) obtained with this Gaussian fit have then

FIG. 2.—*Continued*

been used to generate a "Gaussian cube" that has been subtracted from the data, leaving the residual anomalous gas. A second method has been tried to generate the Gaussian cube for the cold disk by fitting half a Gaussian to the high-velocity side of the line profiles. This is based on the assumption that the anomalous gas does not contribute to the high-velocity side of the line profile. The obtained half-Gaussian has then been folded on the low-velocity side of the profile and subtracted from the data. The results obtained with the two methods are very similar.

3.1. *The Cold Disk*

The velocity field and the map of the velocity dispersion of the cold disk are shown in Figure 1. The velocity field is regular and symmetric. The velocity dispersion has average values around 9–10 km s^{-1} except in the central region and in the spiral arms, where it reaches values of up to 10–15 km s^{-1} (darker gray scale). After correction for the instrumental resolution, these values are about 1 km s^{-1} lower. In order to determine the kinematical parameters and the rotation curve of NGC 2403, we have performed the standard tilted-ring fit of the velocity field (Begeman 1987). The rings have been fitted with a radial increment of 15″. Points were weighted by the cosine of the azimuthal angle with respect to the major axis. In the determination of the central position and the systemic velocity only the rings with radii smaller than 13 kpc were considered. The values derived for the position of the center and for the systemic velocity are reported in Table 3. While keeping these parameters fixed, we proceeded to fit the position and inclination angles. The position angle (Fig. 9) shows a clear deviation from the
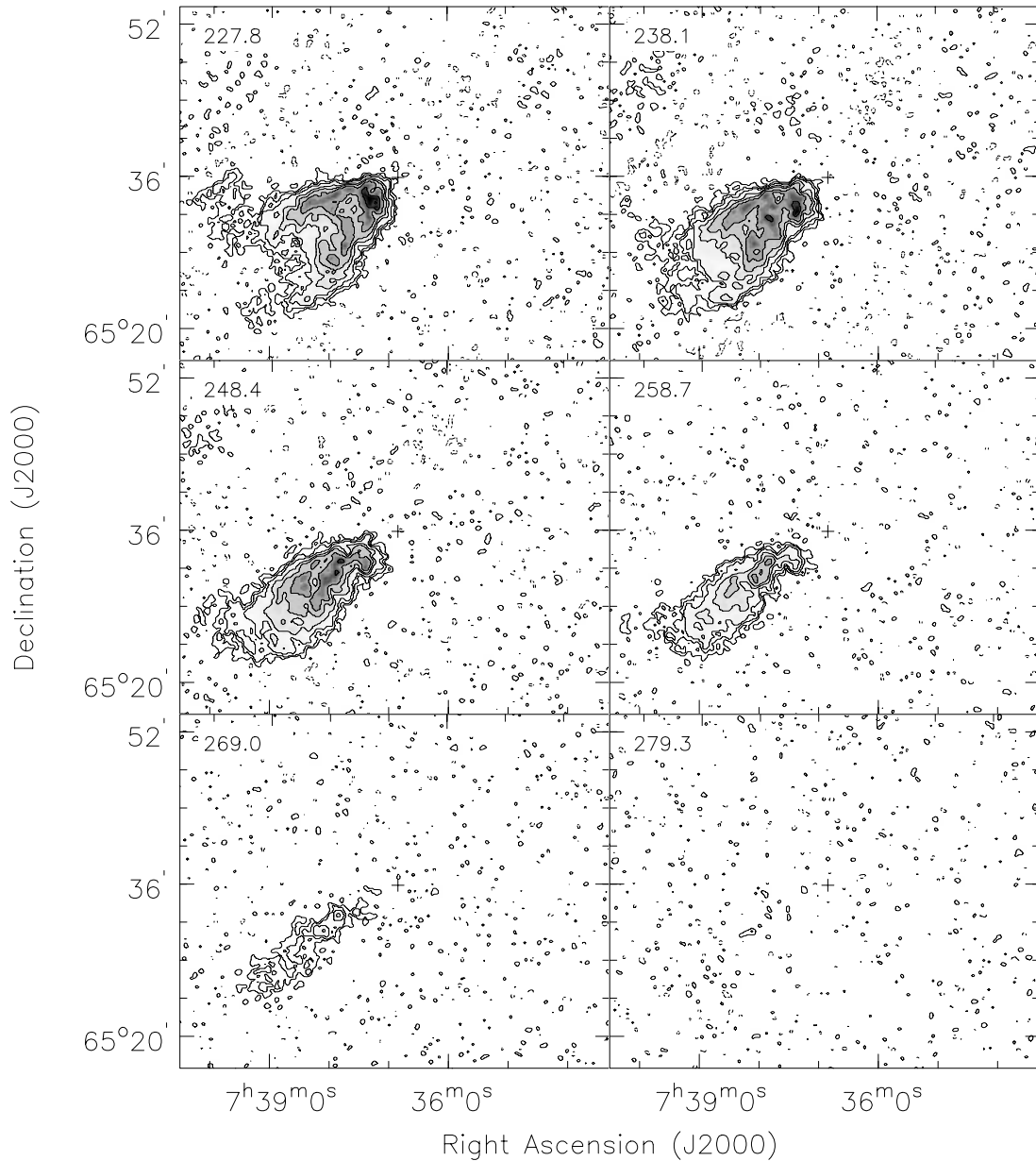
FIG. 2.—*Continued*

mean value in the central region between 2 and 4 kpc and remains constant out to about 15 kpc, where it starts decreasing in the region of the warp. The inclination angle shows variations in the central region around a mean value of about 61°. Then it rises to more than 65° beyond 15 kpc. The mean (error weighted) values for the position and the inclination angles were derived between 4 and 15 kpc and resulted in 124°.5 ± 0°.6 and 62°.9 ± 2°.1, respectively. The values obtained by Sicking (1997) were 123°.9 and 60°.9, respectively, while Begeman (1987) found 122°.5 and 60°.2. The lower values for the inclination angle found by these authors agree with the value we get considering only the inner regions (radii ≤ 10 kpc) of the disk.

While keeping the other parameters fixed, the rotation curve was derived separately for the approaching and receding side of the galaxy, as shown in Figure 9 (*top left*). The

line shows the rotation curve obtained by Begeman (1987). Points beyond 20 kpc were determined using the velocity field at 30″ resolution. Because of the large deviations of position and inclination angles from their mean values beyond 20 kpc, they were left free to vary in the fit. The rotation curves for the two sides indicate a good overall symmetry except for the regions beyond 16 kpc, where the approaching side has velocities 5–10 km s^{-1} higher than the receding one.

Figure 9 also shows the radial column density fitted with an exponential law for radii larger than 4 kpc (the inferred H I scale length is 5.7 ± 0.1 kpc) and the velocity dispersion derived with the formula $\sigma^2_{disp} = \sigma^2_{obs} + \sigma^2_{instr}$, where σ_{instr} is the instrumental velocity resolution ($\simeq 2 \times$ channel separation) and σ_{obs} is the σ of the Gaussian function fitted to the clipped line profile. The derived velocity dispersion
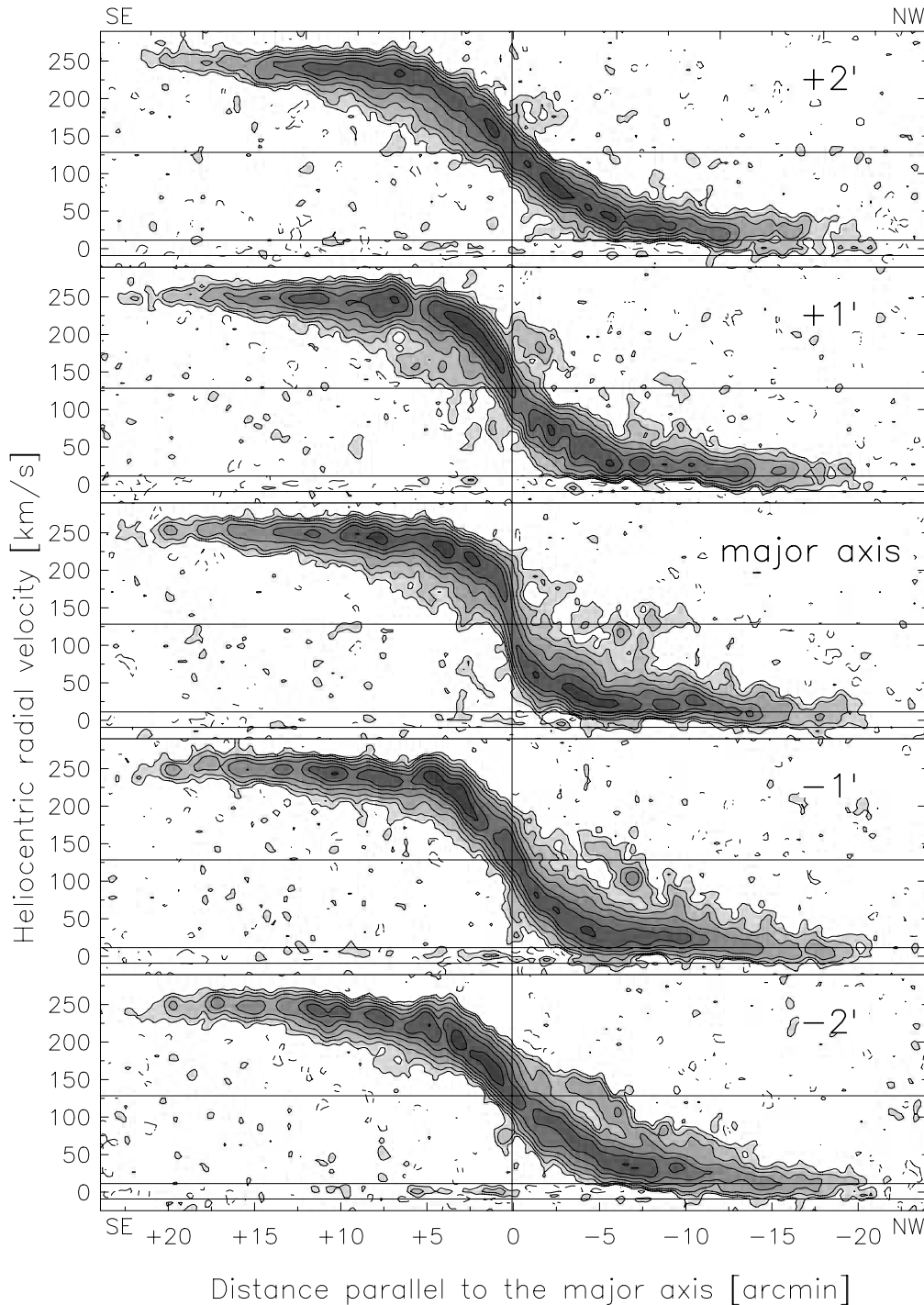
FIG. 3.—Position-velocity diagrams (30″ resolution, Hanning-smoothed) parallel to the major axis of NGC 2403 (P.A. = 124°.5; see Fig. 5). The central panel is the *p-v* plot along the major axis itself. The +1′, +2′ are from cuts taken northeast, respectively, at 1′ and 2′ from the center of the galaxy. The −1′, −2′ are located southwest (1′ is ∼1 kpc). The left side of the diagram corresponds to the southeast side of the galaxy. The central horizontal line shows the systemic velocity; the two lower lines mark the channel maps contaminated by emission from the Milky Way. Contours are −0.45, 0.45, 1, 2, 4.5, 10, 20, 45 mJy beam^{-1}.

shows a decrease from the central values of ∼12 km s^{-1} to values of ∼8 km s^{-1} in the outer regions.

3.1.1. *The Mass Model*

The rotation curve of NGC 2403 was derived again by applying the tilted-ring fitting to the velocity field of the whole galaxy. For points beyond 20 kpc we again used the smoothed data cube with no fixed position and inclination angles. As an estimate of the errors, we took the difference in velocity between the approaching and receding side. We have subsequently performed the standard analysis of the rotation curve with the decomposition into three mass components (Begeman 1989): the stellar disk, the gas disk, and the dark matter halo. No stellar bulge is visible in the optical luminosity profile (Kent 1987). For the stellar disk we have
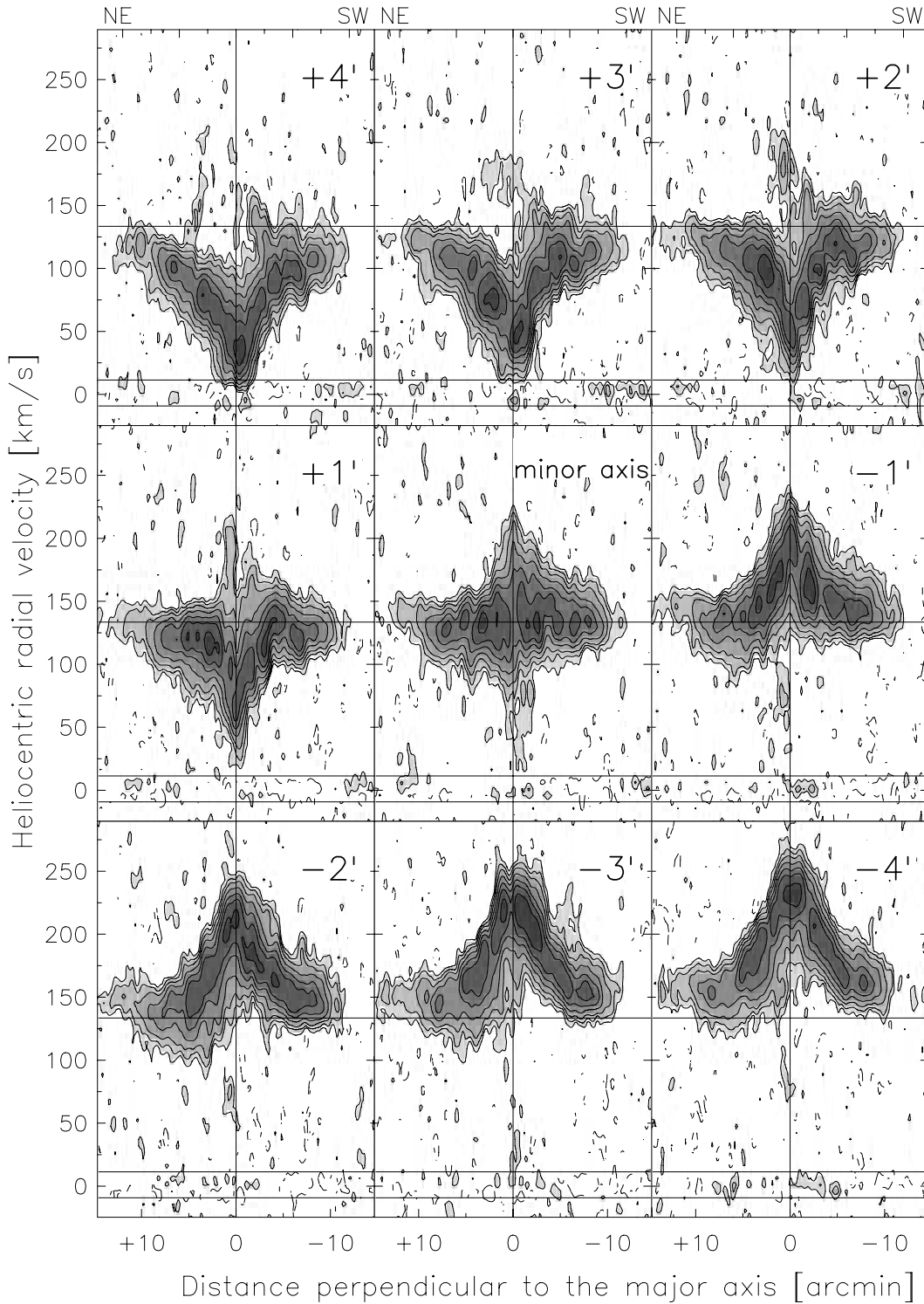
Fig. 4.—Position-velocity diagrams (30″ resolution, Hanning-smoothed) parallel to the minor axis of NGC 2403 (P.A. = 34°.5; see Fig. 5). The central panel is the *p-v* plot along the minor axis. The +1′, +2′... are from cuts taken northwest respectively at 1′ and 2′... from the center of the galaxy. The −1′, −2′... are located southeast. The left side of the diagram corresponds to the northeast side of the galaxy. The central horizontal line shows the systemic velocity; the other two horizontal lines mark the channels contaminated by H I emission from the Milky Way. Contours are −0.45, 0.45, 1, 2, 4.5, 10, 20, 45 mJy beam^{-1}.

taken the brightness profile published by Kent (1987), while for the H I profile we multiplied our data by a scale factor of 1.4 to take into account the helium abundance. We assumed a value of 0.4 kpc for the scale height of the stellar layer (van der Kruit & Searle 1981) and 0.2 kpc for the gas layer Sicking 1997). The dark matter halo was modeled with the

spherically symmetric density distribution $\rho(R) = \rho_0(1 + R/R_0)^{-2}$, where ρ_0 is the central density and R_0 is the core radius.

In Figure 10 we show four different fits. The maximum disk model gives a scaling factor (M/L) for the stellar component of 2.3, the "Bottema disk" model (Bottema 1993)
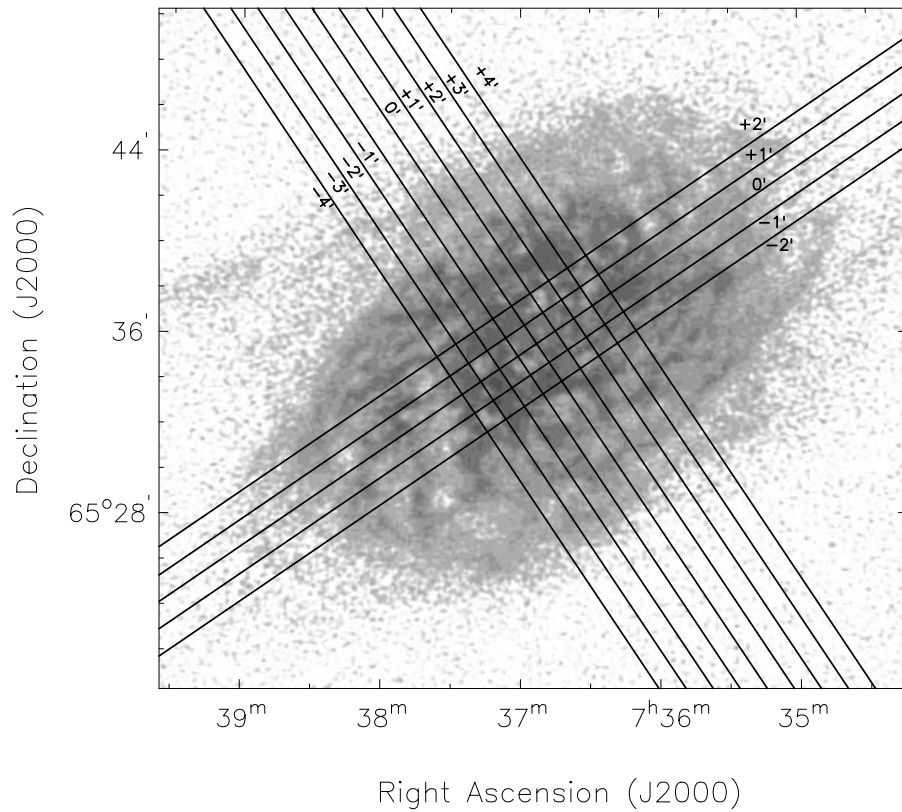
Fig. 5.—Total H I map showing the cuts parallel to the major and the minor axes used for the position-velocity maps displayed in Figs. 3 and 4

has a fixed M/L of 1.4, and the third model is the so-called maximum halo (no stellar disk). The fourth panel shows a model with no dark matter halo and a free scale factor for stars and H I; we obtained an M/L of 2.3 and a value of 9.9 for the H I scaling factor, similar to that found by Hoekstra, Van Albada, & Sancisi (2001). The first three fits are compa-

rable. Note that the last model gives a higher discrepancy in the outer regions than found by Hoekstra et al. 2001. However, this latter produces the best fit of the inner substructures of the rotation curve. The present rotation curve is more extended (about 2 kpc) than that by Begeman (1987) and does not show any sign of declining. The total dynami-
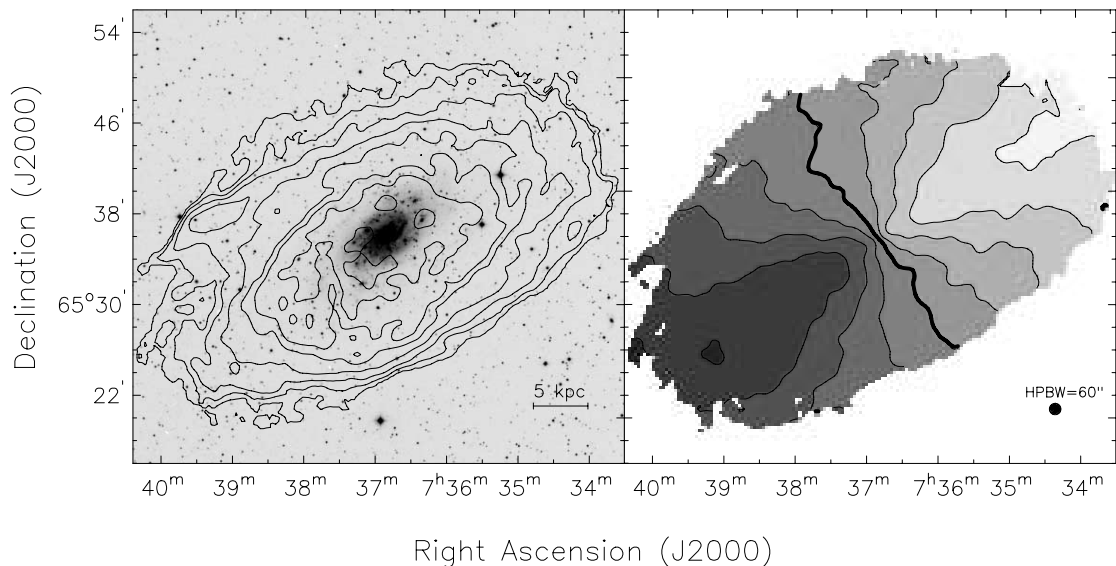

Fig. 6.—Total H I overlaid on the DSS optical image and velocity field for NGC 2403 at low (60″) angular resolution. The presence of the outer warp is visible on the northeast side of the disk. The contours are 2.4, 6.4, 13, 26, 52, 78, 126, 207 × 10^{19} cm^{-2} (the lower level is ≈2 in terms of rms noise). In the velocity field the contours are separated by 30 km s^{-1} and the thicker one marks the systemic velocity (133 km s^{-1}). The receding side is darker.
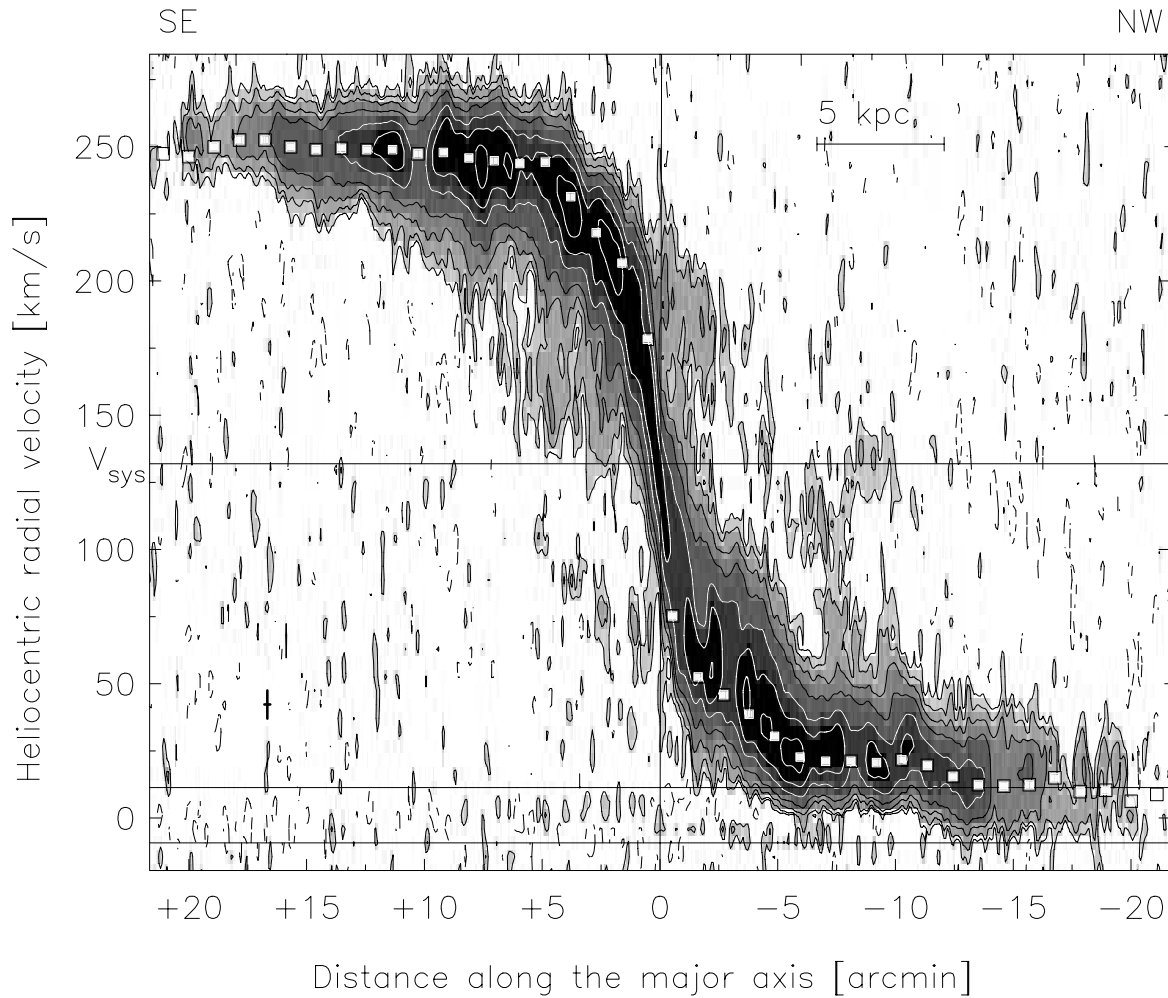
Fig. 7.—Position-velocity diagram (slice ∼1′ wide) along the major axis (P.A. = 124°5) of NGC 2403. The spatial resolution is 15″, and the velocity resolution 10.3 km s^{-1}. The central horizontal line shows the systemic velocity; the other two horizontal lines mark the channels contaminated by H I emission from the Milky Way. Contours are −0.26, 0.26, 0.5, 1, 2, 5, 10, 20 mJy beam^{-1}. The rms noise is 0.17 mJy beam^{-1}. White squares mark the rotation curves for the two sides of the galaxy.

TABLE 3
OPTICAL AND RADIO PARAMETERS FOR NGC 2403

Parameter	NGC 2403	Ref.
Morphological type	Sc(s) III	1
Optical center		
$(\alpha, \delta$ J2000.0)......................	7 36 51.92 65 36 0.6	2
Kinematical center		
$(\alpha, \delta$ J2000.0)......................	7 36 50.66 ± 1.48 65 36 2.2 ± 5.5	3
Distance (Mpc)	3.18	4
L_B $(L_{\odot B})$..................................	$7.9 \pm 0.7 \times 10^9$	5
Disk scale length (kpc)	2.0	6
R_{25} (kpc)	8.2	5
Holmberg radius (kpc)	13.4	7
H I scale length (kpc)	5.7 ± 0.1	3
H I disk radius (kpc)	22.5	3
Systemic velocity (km s^{-1})......	133.2 ± 2.2	3
H I total mass $(M_{\odot})$.................	$3.24 \pm 0.05 \times 10^9$	3
Mean H I inclination (deg)	62.9 ± 2.1	3
Mean P.A. (no warp) (deg).....	124.5 ± 0.6	3
Total mass $(M_{\odot})$......................	$9.5 \pm 0.7 \times 10^{10}$	3

REFERENCES.—(1) Sandage et al. 1981 (2) Gallouët, Heidmann, & Dampierre 1973; (3) this work; (4) Madore & Friedman 1991; (5) de Vaucouleurs, de Vaucouleurs, & Corwin 1976; (6) Wevers, Van der Kruit, & Allen 1986; (7) Holmberg 1958.

cal mass inferred within a galactic radius of 22.5 kpc is $9.4 \pm 0.7 \times 10^{10}$ $M_{\odot}$. This value is consistent with that obtained by Begeman (1987) ($8.4 \pm 0.4 \times 10^{10}$ $M_{\odot}$) for a galactic radius of 20 kpc.

3.2. The Anomalous Gas

Figure 11 shows the p-v diagram for the anomalous gas along the major axis of NGC 2403 after the subtraction of the cold disk. The filled squares show the rotation curve derived for the cold disk. Figure 12 shows the distribution of the anomalous gas overlaid on the optical picture (*left*). Its outer radius is about 15–16 kpc and the total H I mass is ∼3×10^8 $M_{\odot}$ (1/10 of the total H I mass of NGC 2403, 0.3% of the total dynamical mass). For the velocity dispersion of the anomalous gas the data indicate values of 20–50 km s^{-1}.

Where is this anomalous gas located in space with respect to the cold disk? Is it located above the disk in the halo region? The vertical extent of this gas layer is difficult to determine precisely because the inclination of the galaxy is not sufficiently high. Schaap et al. (2000), using a three-dimensional modeling of the gas layer, arrived at possible values for its thickness between 1 and
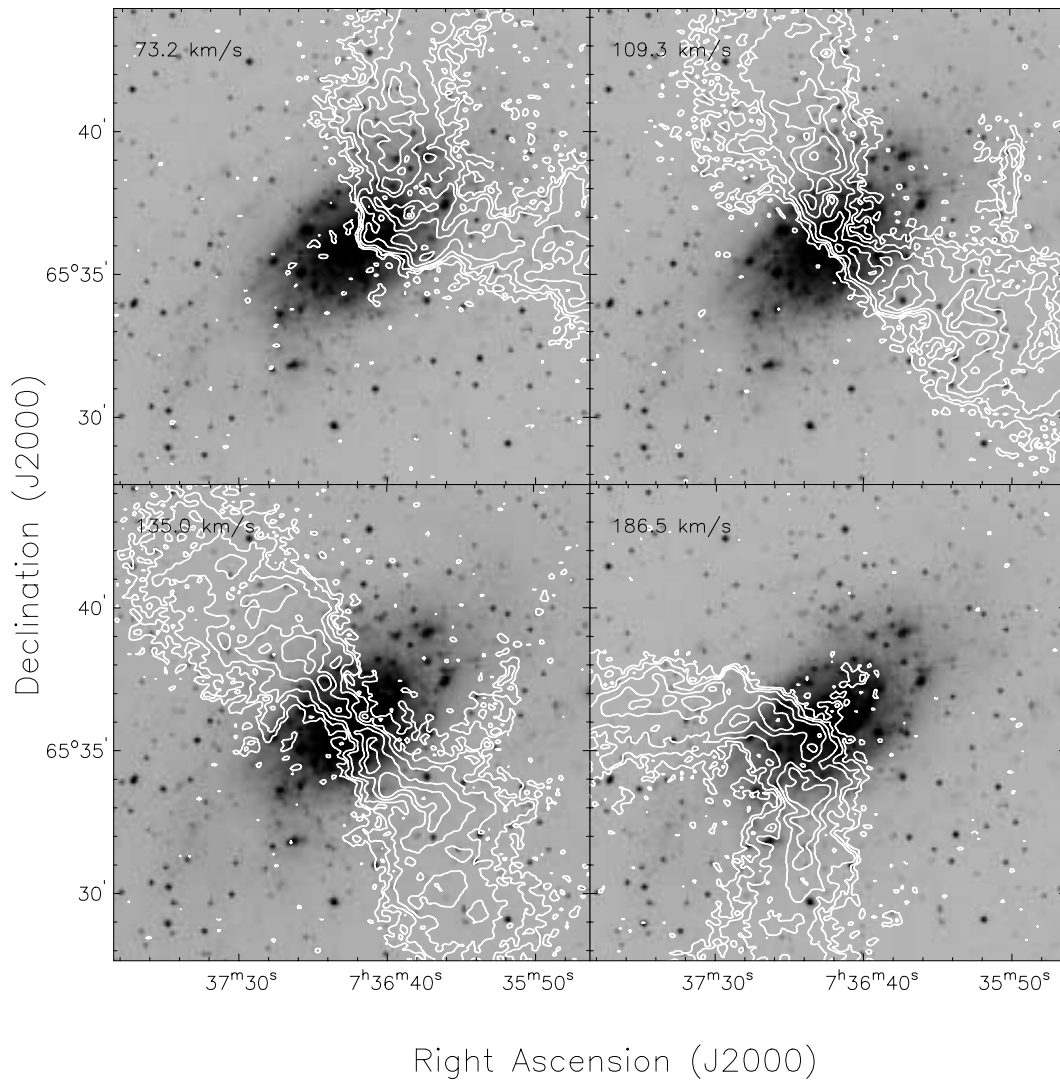
Fig. 8.—Four representative channel maps at 15″ resolution overlapping the optical image of NGC 2403. Contour levels are −0.5, 0.5, 1, 2, 5, 10, 20 mJy beam^{-1}. The rms noise is 0.17 mJy beam^{-1}. The bottom right panel shows the forbidden gas in the northwest side of the galaxy, while the top left panel shows the faint emission of forbidden gas in the southeast side. The other panels show the bright 8 kpc filament in the west side of the H I disk. Note its location outside the bright part of the optical disk.

3 kpc (FWHM). Similar values were found for the edge-on galaxy NGC 891 (Swaters et al. 1997) whose H I "halo" is probably a component similar to the anomalous gas in NGC 2403. A similar modeling performed by us gives an upper limit for the thickness of the anomalous gas of about 3 kpc, while the thickness of the disk is presumably lower than 0.4 kpc (Sicking 1997). Also from a dynamical point of view this separation into two systems of different thicknesses is natural, as the anomalous gas and the cold disk, being collisional systems with separate kinematics, cannot spatially coexist in the same thin layer.

3.2.1. Velocity Field and Radial Motions

Figure 12 (right) shows the intensity-weighted velocity field of the anomalous gas. Clearly the kinematics is dominated, as for the cold disk, by differential rotation. The projected kinematical axes, however, appear to be rotated

counter-clockwise with respect to those of the cold disk. This is more evident for the minor axis (thick line). Furthermore, the two axes are not orthogonal. This is a result of the asymmetric distribution of the anomalous gas already noted in the description of the p-v parallel to the minor axis of the galaxy (§ 2.2.1). A simple explanation is that of an overall inflow of the anomalous gas toward the center of the galaxy (Fraternali et al. 2001).

We have explored the possibility of such a radial flow quantitatively using a tilted-ring fit to the velocity field of the anomalous gas. This was done by keeping the center of the galaxy and the systemic velocity fixed to the values found for the cold disk. The resulting inclination angle is similar to that of the disk, but the position angle, as expected from the counter-clockwise rotation of kinematical axes, turns out to be significantly higher (~131°). Assuming such a rotation of the kinematical axes is indeed due to radial motions, we have included in the tilted-ring model a radial component for the gas velocity. In order to
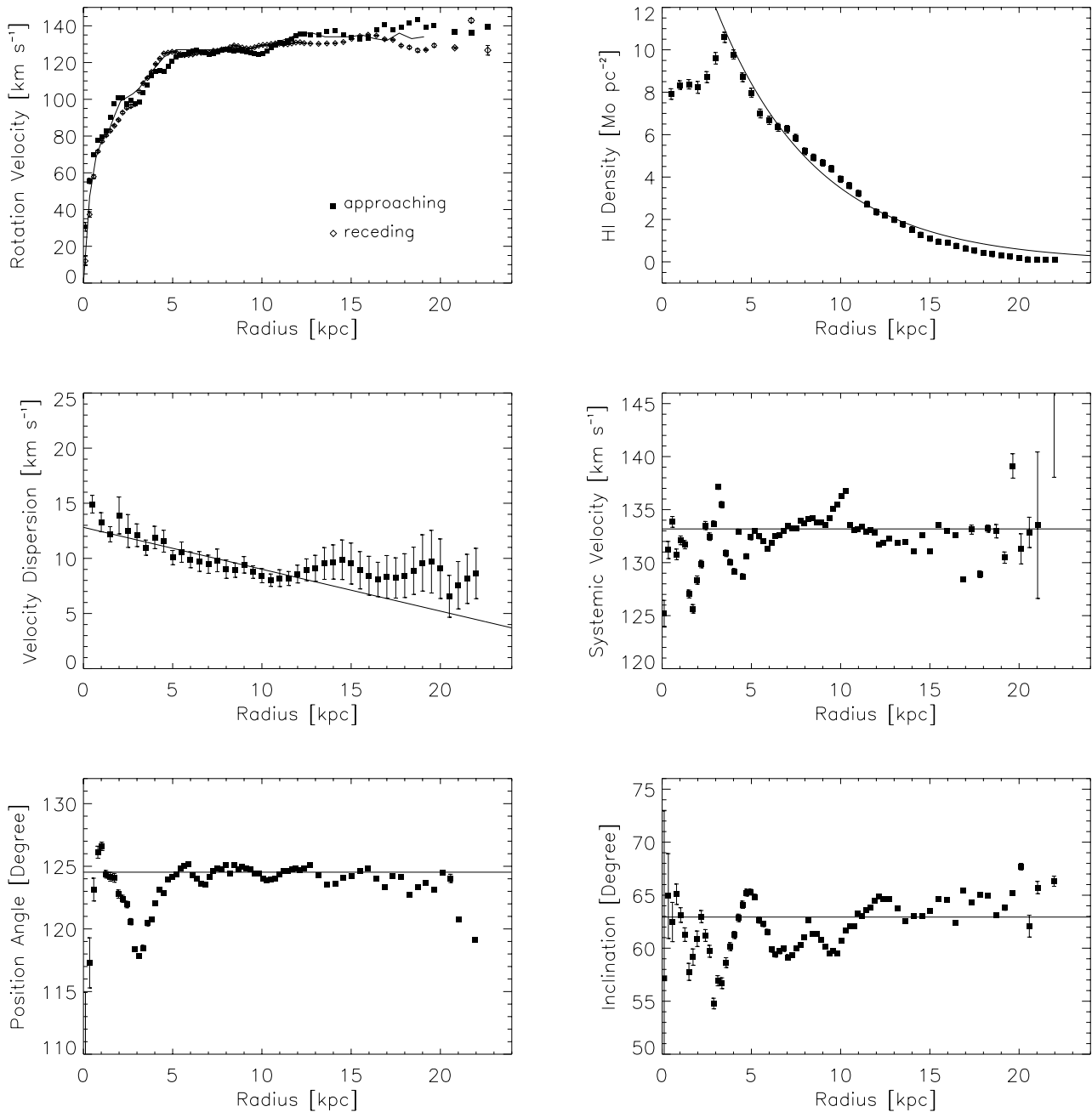
FIG. 9.—Radial profiles of parameters of the tilted-ring model for NGC 2403. In the top left panel the rotation curves obtained for the two sides of the galaxy are shown. The line shows the rotation curve obtained by Begeman (1987).

decide about the sign of such radial motion—inflow or outflow—it is necessary to know which is the near and which is the far side of the galaxy. We have taken the southwest side as the near side of NGC 2403. This is based on the assumption that the spiral arms are trailing and is also supported by the presence of dust absorption features (see optical images in Sandage et al. 1981). Keeping the position angle fixed to the value found for the cold disk (124.5), the fit gives a radial flow velocity of -13.6 ± 1.2 km s^{-1} (the minus sign means inflow) from 4 to 15 kpc.

Is it possible that also the cold disk has a nonzero radial velocity? We tested this possibility by considering both radial velocity and position angle as free parameters in the tilted-ring fit to the velocity field of the cold disk. Figure 13 (right) shows the trend of radial velocity for both the disk and the anomalous gas obtained with this method. The mean values of radial velocity between 4 and 15 kpc are -3.1 ± 0.3 and -16.2 ± 1.1 km s^{-1} for the disk and the anomalous gas, respectively. Thus the velocity field of the cold disk also shows a small distortion that could be explained as a weak radial inflow. However, an alternative and more likely interpretation for this distortion is that of triaxiality of the potential. Indeed, the deviation from circular motion found here is comparable to that found by Schoenmakers, Franx, & de Zeeuw (1997) (about 2 km s^{-1}) with a Fourier analysis of the orbits. Such a weak triaxiality
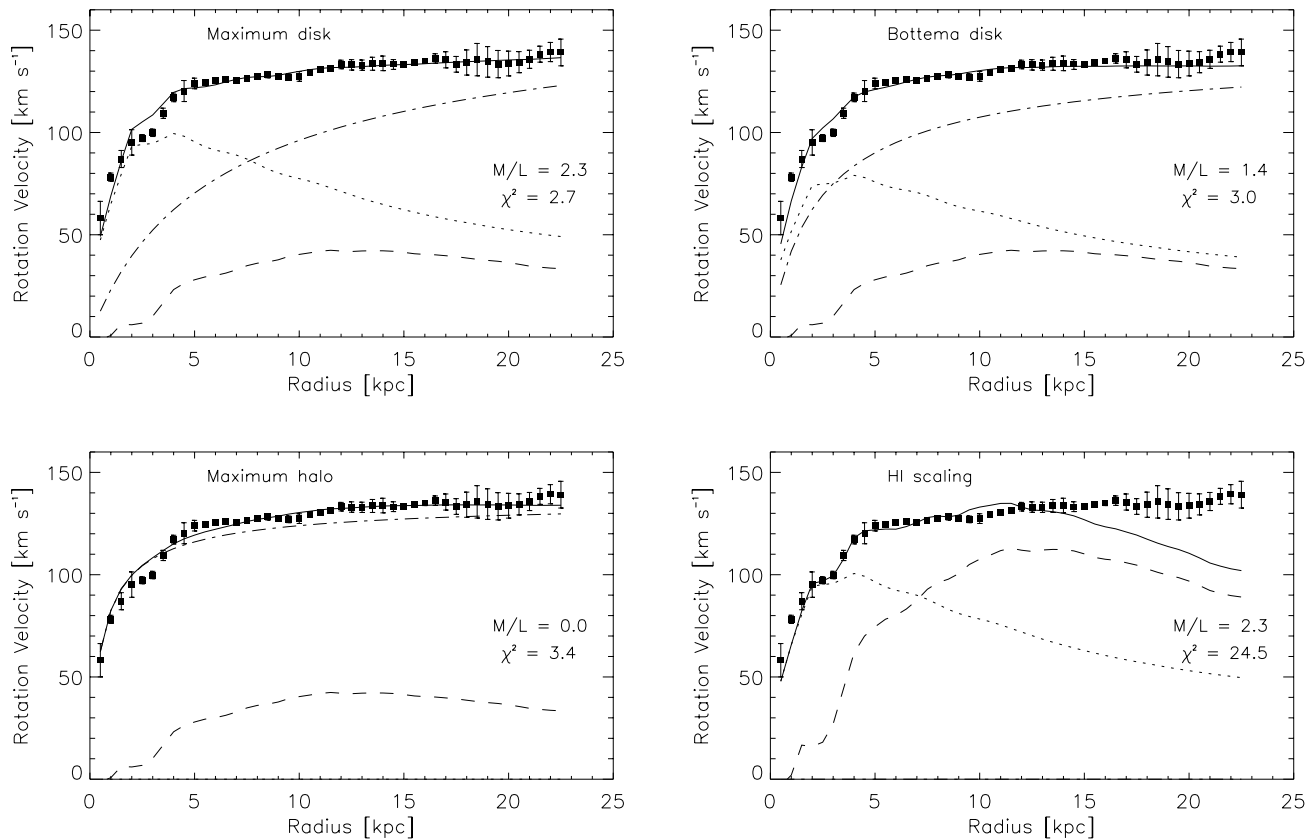
Fig. 10.—Four different mass models for NGC 2403. The filled squares show the observed rotation curve, the contributions by gas (*dashed*), stars (*short dashed*), and DM halo (*long-short dashed*) and the total rotation velocity (*solid*). Values of χ^2 and scaling factor (M/L) of the stellar profile are given as well.

would, instead, be totally insufficient to account for the effect (a factor of 10 greater) observed for the anomalous gas.

Figure 13 also shows the rotation curve of the disk compared with the mean rotation velocity of the anomalous gas. The difference is about 25 km s^{-1} in the outer parts, increasing to 40–50 km s^{-1} in the inner regions. Table 4 summarizes the properties of the H I disk and of the anomalous gas for NGC 2403.

4. SUMMARY AND CONCLUDING REMARKS

We have presented new, deep H I observations of the spiral galaxy NGC 2403. These have been used to study the structure of the gas layer and the dynamics of the system. The main results are briefly summarized here.

A new faint, extended gas component with anomalous velocities has been detected. This H I component (the

" anomalous gas ") shows up in the line profiles as broad wings at velocities lower than rotation and partly also at forbidden (noncircular) velocities. Such wings are not explained by inclination effects, pure thickness, or poor angular resolution but result from the presence of a thick layer of H I, which rotates more slowly than the gas in the plane (see also Schaap et al. 2000).

We have separated the anomalous gas from the thin disk of cold H I, assuming a Gaussian profile for the latter. The anomalous H I has a mass of about $3 \times 10^8 \ M_\odot$ (1/10 of the total H I mass), a mean rotation velocity 25–50 km s^{-1} lower than that of the disk, and a radial inflow of 10–20 km s^{-1}.

The origin of this gas is still a matter of debate. The main issue is whether it is the result of processes taking place in the system itself or whether it could be infall of extragalactic, possibly primordial, gas (see Oort 1970). The overall kinematical pattern of the anomalous gas, its highly coherent structure and its close connection with the disk of NGC 2403 seem to point at an internal origin. Indeed, there may be a close relation with the process of active star formation going on in the disk of NGC 2403 and a galactic fountain type of mechanism may provide the explanation for both its origin and its dynamics. However, the detection of H I at forbidden velocities (more than 130 km s^{-1} from rotation) and the presence of coherent structures with sizes up to 8 kpc, are puzzling. Considering the large velocity dispersion (about 20–50 km s^{-1}) and the lower rotation velocities found for the anomalous H I, it is tempting to describe what we see here in terms of a large asymmetric drift of a thick and clumpy gas layer.

TABLE 4
Comparison between Disk and Anomalous Gas

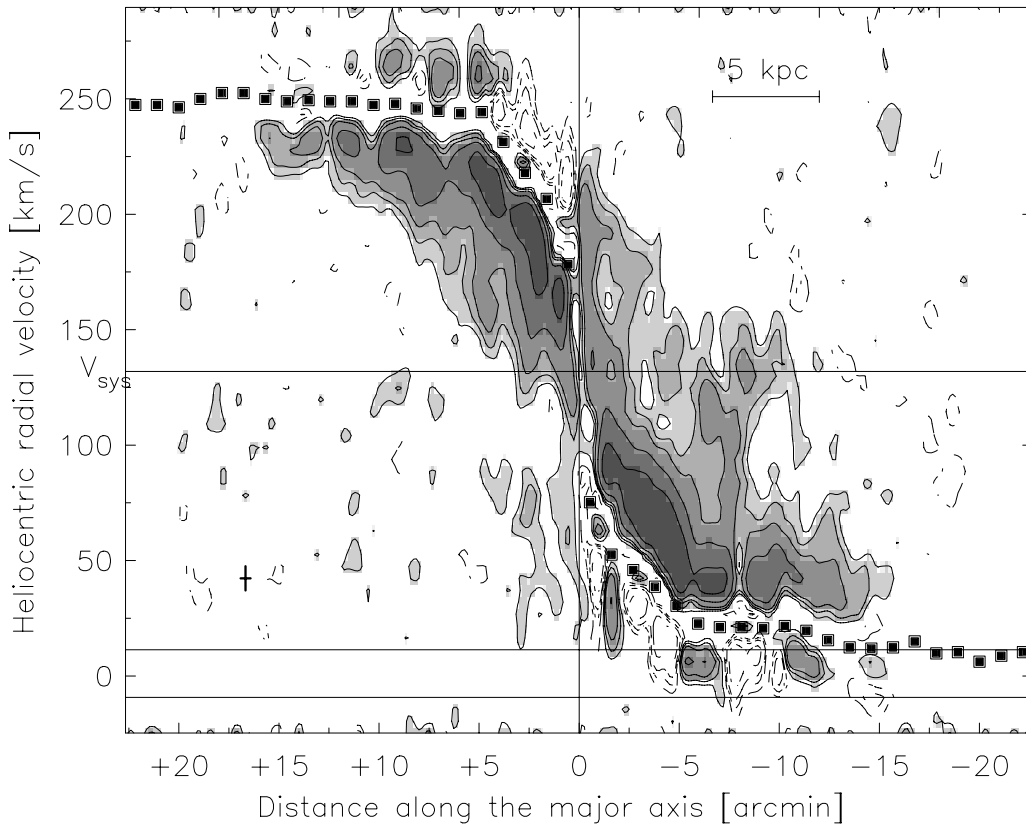| Parameter	Cold Disk	Anomalous Gas
Mass ($M_\odot$)	3×10^9	3×10^8
Diameter (kpc)..................................	46	32
Thickness (kpc)..................................	0.4	<3
Maximum rotation velocity (km s^{-1})...	130	110
Mean radial inflow velocity (km s^{-1}) ...	0–3	10–20
Mean velocity dispersion (km s^{-1}).......	8–12	20–50

Fig. 11.—Position-velocity diagram for the anomalous gas along the major axis of NGC 2403. Contours are 2, 4, 8, 20, 40 in units of rms noise. The filled squares mark the rotation curve of the cold disk.

The results of the present H I observations of NGC 2403 also have interesting implications regarding the high-velocity clouds observed in the Milky Way (Wakker & Van Woerden 1997), whose distances, nature, and origin are still a matter of debate. It is possible that the anomalous H I complexes discovered in NGC 2403 are analogous to the HVCs seen in the Galaxy, or at least to a class of them. Consider, for instance, the 8 kpc filament, the largest structure found in NGC 2403, with a projected velocity difference from the rotation of 60–100 km s^{-1} and an H I mass of about

1×10^7 $M_\odot$. If viewed from inside NGC 2403, it would probably appear to have a large angular size similar to that of some extended HVC complexes, e.g., the well-known complex C (Wakker et al. 1999). To be as massive as the filament in NGC 2403, complex C would have to be as far as 15 kpc from us, compatible with the observational lower limits (Wakker & Van Woerden 1997). Such a distance would also be of the same order as the distance (between 4 and 10 kpc) estimated for complex A (van Woerden et al. 1999), which shows several similarities with complex C. The fact that
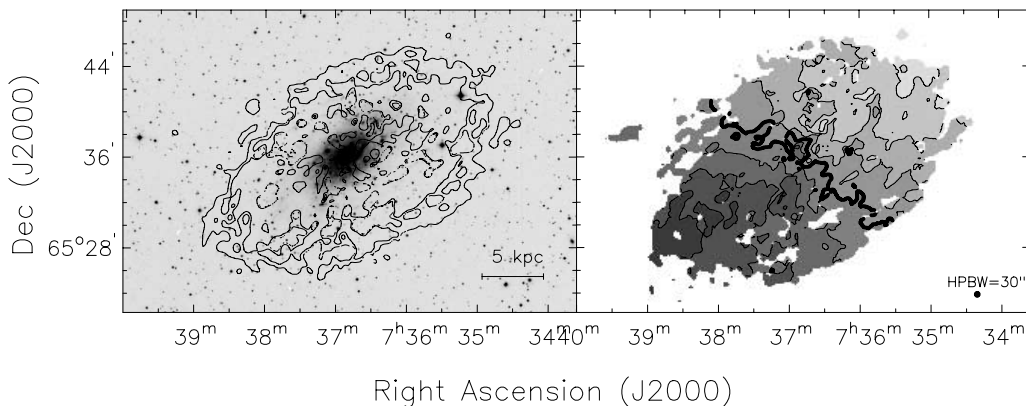

Fig. 12.—Total H I map and weighted mean velocity field of the anomalous gas in NGC 2403. In the left panel the density distribution of the anomalous gas is overlaid on the optical DSS image of the galaxy. The contours are 2, 6, 15 in units of rms noise. In the velocity field (right) the contours are separated by 30 km s^{-1}, and the thick one shows the systemic velocity (kinematical minor axis). Note that this latter is rotated counter-clockwise (by about 20°) with respect to the minor axis of the velocity field of the cold disk shown in Fig. 1.
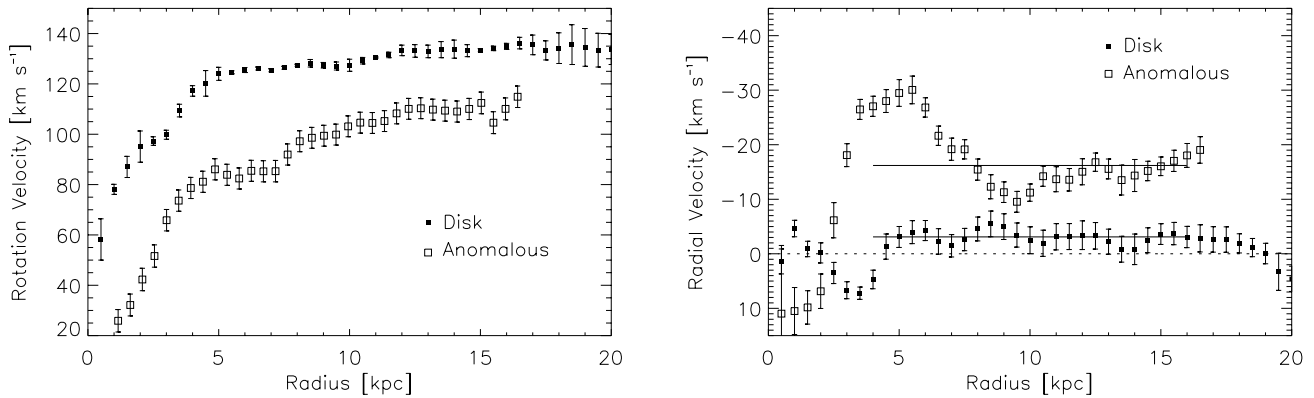
Fig. 13.—Rotation curves (*left*) and radial curves (*right*) for the cold disk (*filled squares*) and for the anomalous gas (*open squares*). The mean values of the radial inflow velocity for the anomalous gas and for the disk (*lines*) are, respectively, 16.2 and 3.1 km s^{-1}.

NGC 2403 is a normal, noninteracting spiral galaxy suggests that the H I features discovered here may be common among spiral galaxies and that, perhaps, they have not been detected yet because of the low sensitivity of previous surveys.

Apart from the investigation of the newly discovered anomalous gas component, the present observations have also been used for the study of the dynamics of NGC 2403. The main results are the finding of an extended, highly asymmetrical warp of the H I outer layer and the derivation of a new rotation curve. This has been analyzed with the standard decomposition technique, and the main results on the disk and the dark matter halo are similar to those already obtained by Begeman (1987).

REFERENCES

Begeman, K. G. 1987, Ph.D. thesis, Univ. Groningen
———. 1989, A&A, 223, 47
Bottema, R. 1993, A&A, 275, 16
Bregman, J. N. 1980, ApJ, 236, 577
Briggs, D. S. 1995, AAS Meeting, 87, 11202
Clark, B. G. 1980, A&A, 89, 377
Cornwell, T. J., Uson, J. M., & Haddad, N. 1992, A&A, 258, 583
de Vaucouleurs, G., de Vaucouleurs, A., & Corwin, H. G. 1976, Second Reference Catalogue of Bright Galaxies (Austin: Univ. Texas Press)
Drissen, L., Roy, J.-R., Moffat, A. F. J., & Shara, M. M. 1999, AJ, 117, 1249
Fraternali, F., Oosterloo, T., Sancisi, R., & van Moorsel, G. 2001, ApJ, 562, L47
Gallouët, L., Heidmann, N., & Dampierre, F. 1973, A&AS, 12, 89
Hoekstra, H., van Albada, T. S., & Sancisi, R. 2001, MNRAS, 323, 453
Holmberg, E. 1958, Medd. Lund Obs. Ser. II, 136
Kamphuis, J. J. 1993, Ph.D. thesis, Univ. Groningen
Kent S. M. 1987, AJ, 93, 816
Madore, B. F., & Freedman, W. L. 1991, PASP, 103, 933
Mashchenko, S. Y., Thilker, D. A., & Braun, R. 1999, A&A, 343, 352
Oort, J. H. 1970, A&A, 7, 381

Puche, D., Westpfahl, D., Brinks, E., & Roy, J.-R. 1992, AJ, 103, 1841
Rots, A. H. 1980, A&AS, 41, 189
Rupen, M. 1998, VLA Sci. Memo., 175
Sancisi, R. 1999, Ap&SS, 269, 59
Sandage, A., Tammann, G. A., & van den Bergh, S. 1981, A Revised Shapley-Ames Catalog of Bright Galaxies, JRASC, 75, 267
Schaap, W. E., Sancisi, R., & Swaters, R. A. 2000, A&A, 356, L49
Schoenmakers, R. H. M., Franx, M., & de Zeeuw, P. T. 1997, MNRAS, 292, 349
Shapiro, P. R., & Field G. B. 1976, ApJ, 205, 762
Sicking, F. J. 1997, Ph.D. thesis, Univ. Groningen
Swaters, R. A., Sancisi, R., & van der Hulst, J. M. 1997, ApJ, 491, 140
van der Hulst, T., & Sancisi, R. 1988, AJ, 95, 1354
van der Kruit, P. C., & Searle, L. 1981, A&A, 95, 105
van Woerden, H., Schwarz, U. J., Peletier, R. F., Wakker, B. P., & Kalberla, P. M. W. 1999, Nature, 400, 138
Wakker, B. P., et al. 1999, Nature, 402, 388
Wakker, B. P., & van Woerden H. 1997, ARA&A, 35, 217
Wevers, B. M. H. R., Van der Kruit, P. C., & Allen, R. J. 1986, A&AS, 66, 505